Model-based analysis of reflectance and fluorescence spectra for *in vivo* detection of cervical dysplasia and cancer

Crystal Redden Weber
Rice University
Department of Chemistry
Houston, Texas 77005

Richard A. Schwarz
Rice University
Department of Bioengineering
Houston, Texas 77005

E. Neely Atkinson
University of Texas M.D. Anderson Cancer Center
Department of Biostatistics
Houston, Texas 77030

Dennis D. Cox
Rice University
Department of Statistics
Houston, Texas 77005

Calum MacAulay
British Columbia Cancer Research Centre
Department of Cancer Imaging
Vancouver, British Columbia V5Z 1 L3, Canada

Michele Follen
University of Texas M.D. Anderson Cancer Center
Department of Gynecologic Oncology
Houston, Texas 77030

Rebecca Richards-Kortum
Rice University
Department of Bioengineering
Houston, Texas 77005

Abstract. Development, validation, and implementation of an analytical model to extract biologically and diagnostically relevant parameters from measured cervical tissue reflectance and fluorescence spectra are presented. Monte Carlo simulations of tissue reflectance are used to determine the relative contribution of the signal from the epithelium and stroma. The results indicate that the clinical probe used collects a majority of its reflectance signal from the stroma; therefore, a one-layer analytical model of reflectance is used. Two analytical approaches to calculate reflectance spectra are compared to Monte Carlo simulations, and a diffusion theory-based model is implemented. The model is validated by fitting spectra generated from Monte Carlo simulations and comparing the input and output parameters. Median agreement between extracted optical properties and input parameters is 10.6%. The reflectance model is used together with an analytical model of tissue fluorescence to extract optical properties and fluorophore concentrations from 748 clinical measurements of cervical tissue. A diagnostic algorithm based on these extracted parameters is developed and evaluated using cross-validation. The sensitivity/specificity of this algorithm relative to the gold standard of histopathology per measurement are 85/51%; this is comparable to accuracy reported in other studies of optical technologies for detection of cervical cancer and its precursors. [DOI: 10.1117/1.3013307]

Keywords: diffuse reflectance spectroscopy; fluorescence spectroscopy; cancer diagnosis.

Paper 08196 received Jun. 25, 2008; accepted for publication Sep. 16, 2008; published online Nov. 10, 2008.

1 Introduction

Optical techniques offer the ability to noninvasively detect spectral alterations associated with morphological and biochemical changes that occur in tissue during neoplastic transformation and progression. Many groups have shown that diffuse reflectance and fluorescence spectra can be used to detect precancer in the cervix and other organ sites.[1–10] A recent paper reviewed 26 studies that reported diagnostic algorithms based on diffuse reflectance spectra, fluorescence spectra, or the combination; approaches that combine reflectance and fluorescence spectra offer the advantage of monitoring morphologic changes using reflectance spectra and biochemical changes using fluorescence spectra, and generally result in higher diagnostic accuracy.[11]

A variety of empirical methods have been used to reduce the dimensionality of tissue fluorescence and reflectance spectra to develop classification algorithms for detection of neoplasia.[1,6,9,12–16] Physically based models have also been used to extract tissue spectroscopic parameters for use in classification algorithms.[7,17–20] Although diagnostic performance is typically similar for physical and empirical methods, physical models give insight into the changes occurring in the tissue that can be probed spectroscopically. Accurate extraction of optical properties from the *in vivo* spectra could perhaps provide better diagnostic accuracy and can potentially provide

Address all correspondence to Rebecca Richards-Kortum, Rice University, Department of Bioengineering, Houston Texas 77005. E-mail: rkortum@rice.edu

1083-3668/2008/13(6)/064016/10/$25.00

insight into understanding which precancerous lesions will progress and which can be left untreated.

The goal of this paper is to develop and evaluate a physically based model to analyze fluorescence and reflectance spectra of normal and neoplastic cervical tissue. We have previously reported an analytical model to extract cervical tissue optical properties from fluorescence spectra.[22] The development of an analytical model to analyze both cervical tissue fluorescence and reflectance offers several important advantages. The combination of both techniques offers the opportunity to improve diagnostic performance. In addition, reflectance spectra can be analyzed to determine tissue absorbance and scattering properties, reducing the number of free model parameters which are subsequently needed to analyze fluorescence data.

In this paper, we evaluate several reflectance-based models together with our fluorescence model to analyze clinical spectra of normal and neoplastic cervical tissue. A number of analytical models have been developed to describe tissue reflectance. Many are based on diffusion theory, despite its known limitations in tissue at short source-detector separations as well as the finite range of optical properties at which it is valid.[18] Sun et al. developed a diffusion-based reflectance model that extracts tissue optical properties from normalized spectra and tested it using data obtained at various source-detector separations.[17] Zonios et al. applied a diffusion-based reflectance model to analyze reflectance data from human adenomatous colon polyps *in vivo*.[7] In addition to diffusion-based models, higher-order approximations have been proposed. Hull and Foster proposed a model using the P_3 approximation to the Boltzmann transport equation as well as a hybrid diffusion-P_3 approximation (P_3-Hybrid).[18] This approximation expands the Boltzman transport equation in terms of Legendre polynomials. The P_k approximation refers to truncating the expression after the kth polynomial; diffusion theory is formally the P_1 approximation. Palmer and Ramanujam developed a Monte Carlo–based inverse reflectance model and applied it to *ex vivo* human breast tissue samples.[19] Reif et al. developed an empirical model for reflectance based on Monte Carlo (MC) simulations and tissue phantom experiments.[20]

We initially performed MC simulations of cervical tissue reflectance to determine whether cervical tissue reflectance could be described using a one- or two-layer geometry. We then compared the results of the P_3-Hybrid model proposed by Hull and Foster[18] and the diffusion-based model used by Sun et al.[17] to the results of MC simulations to determine the level of complexity needed to accurately extract optical properties from diffuse reflectance spectra of cervical tissue. Finally, we combined the resulting analytical model of tissue reflectance together with our analytical model of tissue fluorescence to create an adjoint model that could be used to extract tissue optical properties from measurements of tissue fluorescence and reflectance. This inverse adjoint model was applied to *in vivo* clinical data from 330 patients, and the diagnostic performance of the algorithm based on the extracted parameters is assessed.

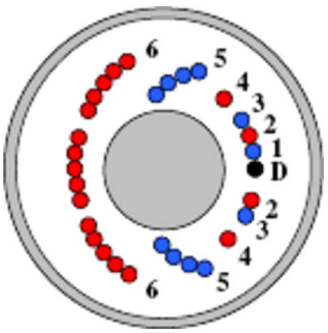

Fig. 1 Diagram of the fiber optic probe used to measure the *in vivo* fluorescence and reflectance spectra. The fluorescence is collected through the large central region, and the reflectance is collected at six source-detector separations at distances from the detector 0.25 mm (1, referred to as SD0), 0.5 mm (2, referred to as SDa), 0.75 mm (3, referred to as SDb), 1.1 mm (4, referred to as SD1), 2.1 mm (5, referred to as SD2), and 3.0 mm (6, referred to as SD3).

2 Methods

2.1 *Overview*

Cervical tissue is comprised of an epithelial layer and an underlying stromal layer. Figure 1 shows the fiber optic probe geometry used to collect clinical measurements of cervical tissue. Fluorescence measurements are obtained through a central channel of the probe, while reflectance measurements are obtained at several different source-detector separations, ranging from 250 μm to 3 mm. The fiber optic probe configuration determines the depth of tissue that is interrogated. We have shown previously that tissue fluorescence collected with this device samples fluorescence contributions from both the epithelium and the stroma. Monte Carlo simulations were performed to determine the fraction of reflectance signal produced in the epithelium and stroma for this probe geometry. Next, two different reflectance models were compared to the results of the MC simulations to determine what level of complexity is needed to describe the data collected clinically. Finally, the previously developed two-layer fluorescence model was combined with the reflectance model chosen to extract optical properties from clinical data.

2.2 *Model Input Parameters*

Cervical tissue was modeled as a 300-μm-thick epithelial layer above a semi-infinite stromal layer. Wavelength-independent scattering anisotropy values of 0.97 and 0.88 were used for the epithelium and stroma, respectively. The scattering and absorption coefficients for squamous normal cervical tissue were used as described in Ref. 21, except that a hemoglobin oxygen saturation value of 85% was assumed. The scattering and absorption coefficients for high-grade precancer are based on results in Ref. 22. The scattering in the epithelium is increased by a factor of three relative to normal tissue for high-grade precancer, and the scattering in the stroma is decreased by a factor of 0.75 relative to normal tissue. The absorption in the epithelium is unchanged from that in normal tissue for modeling high-grade precancer, but the absorption in the stroma is increased by a factor of two relative to that of normal tissue. Figure 2 shows the resulting wavelength-dependent absorption and scattering coefficients

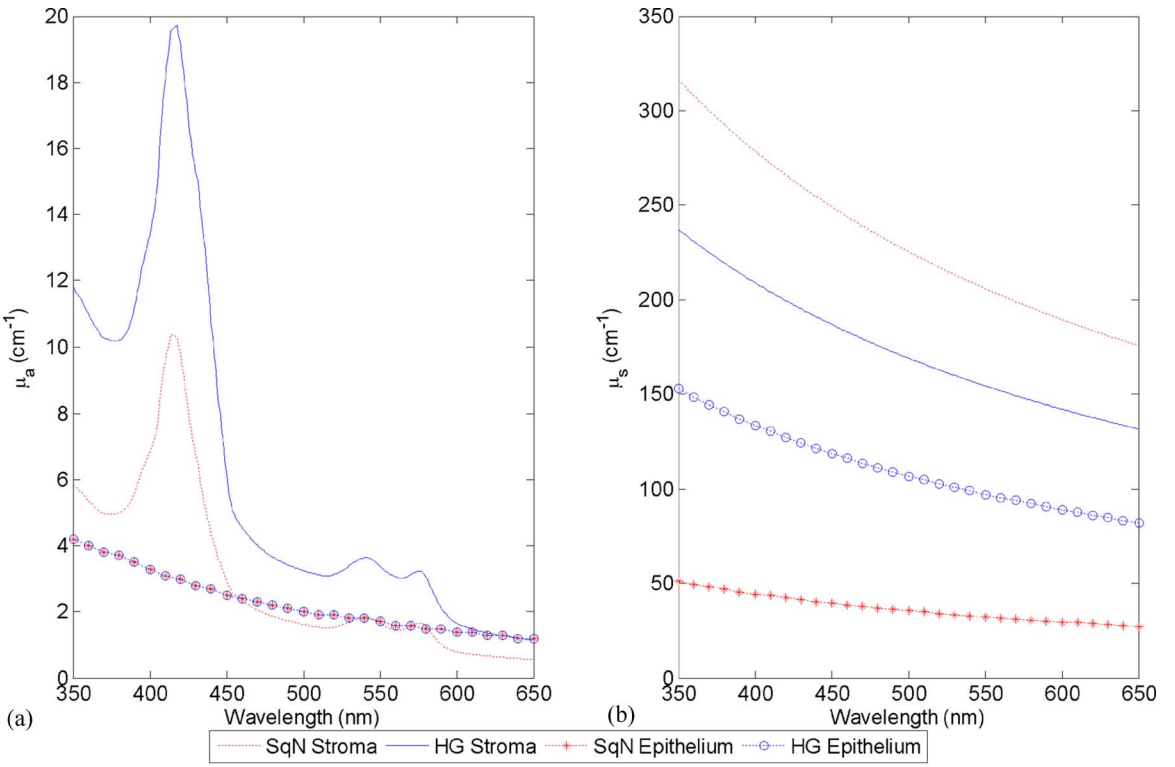

Fig. 2 Squamous normal (SqN) and high grade (HG) tissue optical properties used as input for modeling: (a) absorption coefficient and (b) scattering coefficient

used to model squamous normal cervical tissue and high-grade cervical precancer. These values were used as input to both analytical models of reflectance and MC simulations. The input parameters do not take into account the time-dependent effect of acetic acid application that has been described by Balas.[23] The changes that can occur to the epithelial scattering coefficient over time due to acetic acid application do not have a substantial effect on the reflectance spectrum measured by our device because most of the signal is from the stromal layer.

2.3 *MC Model*

The fixed-weight, multilayered MC code has been previously described and validated by Arifler et al.[21] The MC simulations use typical optical properties of normal and high-grade cervical tissue: absorption coefficient (μ_a), scattering coefficient (μ_s), and anisotropy (g). Monte Carlo simulations were carried out for normal tissue and high-grade precancer, modeling tissues both with a two-layer geometry, with a thin epithelial layer on top of the underlying stroma, and a one-layer geometry consisting of only a stromal layer.

2.4 *Diffuse Reflectance Models*

2.4.1 *Diffusion theory*

The diffusion theory model used the formulation presented in Ref. 17. Figure 3 shows the boundary-mismatched two-dimensional (2-D) semi-infitine homogeneous tissue model used in. Ref. 17. The following expression for the detected reflectance, $R_d(r)$, is used for the forward model:

$$R_d(r) = \frac{a'}{4\pi}\left[\frac{1}{\mu_t'}\left(\mu_{eff}+\frac{1}{r_1}\right)\frac{e^{-\mu_{eff}r_1}}{r_1^2}+\left(\frac{1}{\mu_t'}+2z_b\right)\times\left(\mu_{eff}+\frac{1}{r_2}\right)\frac{e^{-\mu_{eff}r_2}}{r_2^2}\right]. \quad (1)$$

The transport albedo is defined as $a'=\mu_s'/(\mu_a+\mu_s')$, where $\mu_s'=\mu_s(1-g)$ and g is the anisotropy. The total interaction coefficient is $\mu_t'=\mu_a+\mu_s'$. The effective attenuation coefficient is $\mu_{eff}=\sqrt{3\mu_a(\mu_a+\mu_s')}$. The distance from the scattering source to the detector is $r_1=\sqrt{(z-z_0)^2+r^2}$, where z is the distance into the tissue from the surface, and z_0 is the depth of

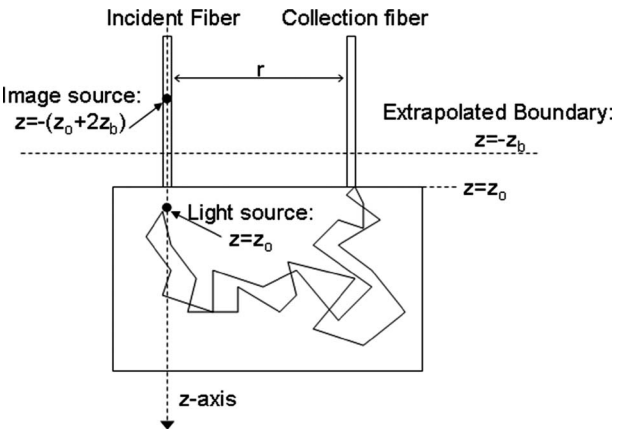

Fig. 3 Diagram of the tissue model used in Ref. 17.

the scatterer. The corresponding distance to the image source is $r_2=\sqrt{(z+z_0-2z_b)^2+r^2}$. z_b is the distance from the tissue surface to the extrapolated boundary and is defined as $z_b=2AD$, where $A=(1-r_d)/(1+r_d)$, $r_d=-1.44n_{rel}^{-2}+0.71n_{rel}^{-1}+0.668+0.0636n_{rel}$, and $n_{rel}=n_{inside}/n_{outside}$, the ratio of refractive indices. The diffusion constant is defined as $D=1/3(\mu_a+\mu_s')$.

2.4.2 P_3-*hybrid approximation*

The reflectance expression used for the P_3-Hybrid forward model, derived in Ref. 18, is $R_d(r;z_0)=[C_\phi\phi_{G_{EBC,asymptotic}}(r;z_0)+C_j j_{z_{EBC}}(r;z_0)](A_{detector})$. The detected reflectance is modeled as the sum of the fluence and flux with appropriate coefficients multiplied by the area of the detector used where

$$\phi_{G_{EBC,asymptotic}}=\frac{1}{4\pi D}\left(\frac{e^{-\mu_{eff}\sqrt{z_0^2+r^2}}}{\sqrt{z_0^2+r^2}}-\frac{e^{-\mu_{eff}\sqrt{(z_0+2z_b)^2+r^2}}}{\sqrt{(z_0+2z_b)^2+r^2}}\right)$$

and

$$j_z=\frac{1}{4\pi}\left[z_0\left(\frac{1}{\sqrt{z_0^2+r^2}}+\mu_{eff}\right)\left(\frac{e^{-\mu_{eff}\sqrt{z_0^2+r^2}}}{\sqrt{z_0^2+r^2}}\right)+(z_0+2z_b)\times\left(\frac{1}{\sqrt{(z_0+2z_b)^2+r^2}}+\mu_{eff}\right)\left(\frac{e^{-\mu_{eff}\sqrt{(z_0+2z_b)^2+r^2}}}{\sqrt{(z_0+2z_b)^2+r^2}}\right)\right].$$

The variables are all defined in the same way as for the diffusion theory except for A, the internal reflectance dependent constant. In the P_3-Hybrid model, $A=(1+R_{eff})/(1-R_{eff})$, where

$$R_{eff}=\frac{R_\phi+R_j}{2-R_\phi+R_j},\quad R_\phi=\int_0^{\pi/2}2\sin\theta\cos\theta R_{Fresnel}(\theta)d\theta,$$

and

$$R_j=\int_0^{\pi/2}3\sin\theta\cos^2\theta R_{Fresnel}(\theta)d\theta$$

where $R_{Fresnel}(\theta)$ is the Fresnel reflection coefficient.

2.4.3 *Fluorescence model*

The fluorescence model used has been previously described in detail in Ref. 22. Fluorescence spectra measured at four excitation wavelengths, 340, 350, 360, and 370 nm, are fit to an analytic expression for tissue fluorescence to extract optical properties of the tissue. The extracted parameters include the concentration of fluorophores reduced nicotinamide adenine dinucleotide (NADH), keratin, flavin adenine dinucleotide (FAD), and three types of collagen crosslinks, the scattering coefficient of the epithelium, the stromal hemoglobin and protein concentrations, the intensity and slope of the scattering coefficient of the stroma, and the hemoglobin oxygen saturation.

2.4.4 *Adjoint inverse model*

The adjoint inverse model allows for extraction of optical properties from the collected reflectance and fluorescence spectra. Tissue reflectance spectra are first fit to an analytical expression to obtain μ_a and μ_s of the stromal layer. Tissue fluorescence spectra are then fit to the analytical expression for fluorescence using the optical properties detected from reflectance spectra and allowing the epithelial scattering and fluorophores concentrations to vary.

3 Instrumentation

A fiber optic point probe was used to measure the reflectance and fluorescence spectra of normal and precancerous regions in 330 patients. Measurements were made of squamous normal tissue, columnar normal tissue, and tissue at the squamous-columnar junction, which may contain both squamous and columnar tissue. The details of the instrumentation used can be found in Ref. 24. Briefly, an arc lamp and filter wheels act as the illumination source and the diffuse reflectance and fluorescence spectra are collected through a fiber probe coupled to a spectrograph and CCD camera. Fluorescence spectra were collected at excitation wavelengths between 300 and 530 nm in 10 nm increments. Reflectance spectra were collected at six different source-detector separations ranging from 0.25 mm to 3.1 mm over a wavelength range of 350–650 nm every 1 nm. The reflectance signal was referenced to a measurement made with the probe placed in the input port of an integrating sphere. Data processing of the raw signal is necessary to ensure that the absolute signal intensity and spectral shape of the reflectance spectrum are accurate. The steps involved include: (*i*) background subtraction, (*ii*) exposure time normalization, (*iii*) wavelength calibration, (*iv*) data smoothing, and (*v*) system response calibration and illumination power normalization.[25]

4 Study Protocol

The study protocol was reviewed and approved by the Institutional Review Boards at the University of Texas M. D. Anderson Cancer Center, Rice University, the British Columbia Cancer Agency, and the University of Texas at Austin. Details of the clinical study are provided in. Ref. 22. Written consent was obtained from all subjects. There are 748 fluorescence and reflectance spectral measurements used in this analysis, and they account for 615 unique sites in 330 patients. This data set is a subset of the data collected in a multicenter phase II clinical trial; our analysis only includes the data measured with one generation of the device used in the trial. The diagnostic categories used for analysis were Normal (normal epithelium, inflammation, metaplasia), LG (low-grade, including atypia, HPV-associated change, grade 1 cervical intraepithelial neoplasia), CIN2 (grade 2 cervical intraepithelial neoplasia), and CIN3+ (grade 3 cervical intraepithelial neoplasia and cancer). Table 1 shows the diagnosis and tissue type statistics for the data analyzed in this study. The classification was performed to discriminate Normal and LG from CIN2 and CIN3+.

5 Statistical Analysis

The training set was split into five groups to perform fivefold cross-validation to estimate the diagnostic performance of the algorithm based on the extracted parameters. Principle components of the measured spectra were also used as features in

Table 1 Statistical breakdown of the data by tissue type and diagnosis.

		Diagnosis				
Number of measurements		Normal	LG	CIN2	CIN3+	All
Tissue type	Squamous	302	56	13	12	383
	Mixed	93	98	53	64	308
	Columnar	46	9	2	0	57
	All	441	163	68	76	748

the algorithm to compare the performance of the physical parameters to empirical parameters. Ten principle components were obtained from the SD1 reflectance spectrum, 10 from the SD3 reflectance spectrum, and 10 from 4 concatenated fluorescence spectra (excitation from 340–370 nm); over 99.9% variance was accounted for in each case. Forward stepwise feature selection based on the highest area under the receiver operating characteristic curve was used to determine the feature set used in the algorithm. Linear discriminant analysis was used for classification.

6 Results

In order to determine whether a one-layer model was adequate to describe the reflectance spectra, both two-layer and one-layer MC simulations were performed for each source-detector separation. The two-layer simulations were performed at emission wavelengths from 350 to 650 nm in 10-nm increments. The one-layer simulations were performed in 1-nm increments from 350 to 650 nm. All the simulations included 10^8 photons, and three simulations were averaged

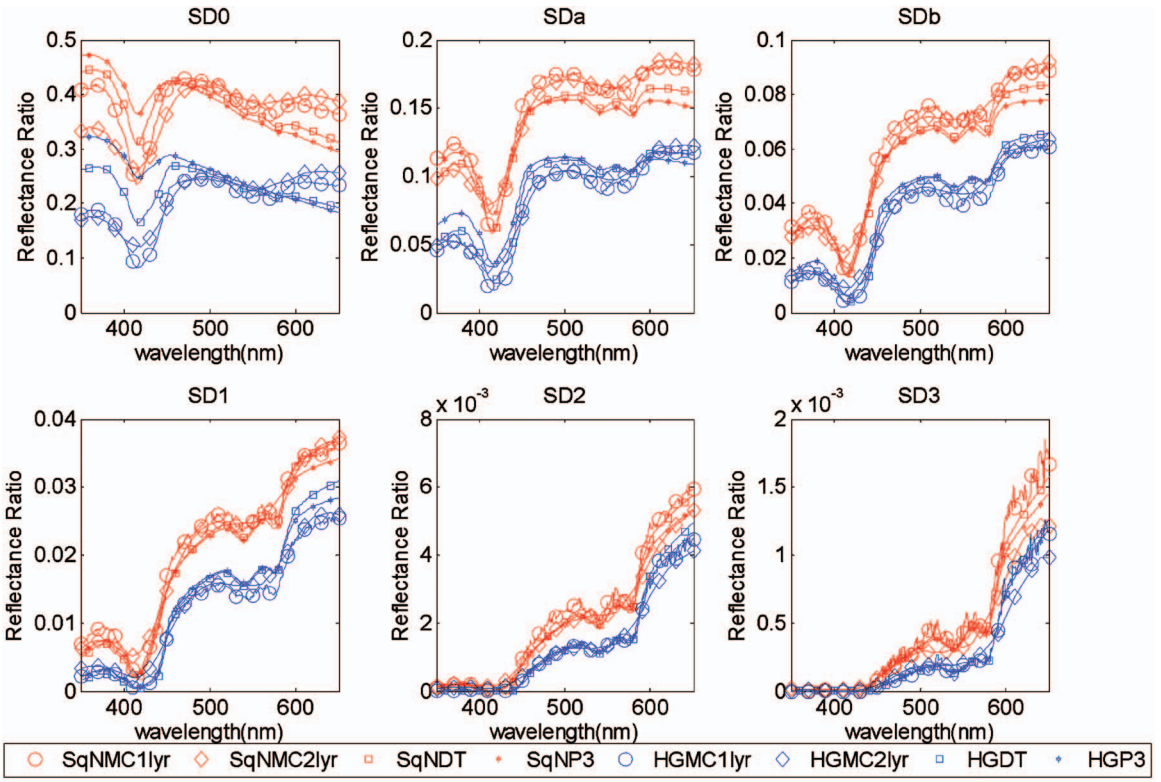

Fig. 4 Diffusion-based forward model, P_3-Hybrid forward model, 1- and 2-layer MC simulations are compared for all source-detector separations. SqNMC1lyr is the one-layer MC simulation for the squamous normal (SqN) input parameters, SqNMC2lyr is the two layer MC simulation for SqN input parameters, SqNDT is the diffusion theory model for SqN input parameters, and SqNP3 is the P_3-Hybrid forward model for the SqN input parameters. The legend entries for the high grade dysplasia (HG) input parameters are defined similarly. The differences are very small except at SD0 for both squamous normal and high grade. Neither diffusion theory nor P_3-Hybrid is expected to be valid at SD0. A one-layer stroma model is sufficient to model the data.

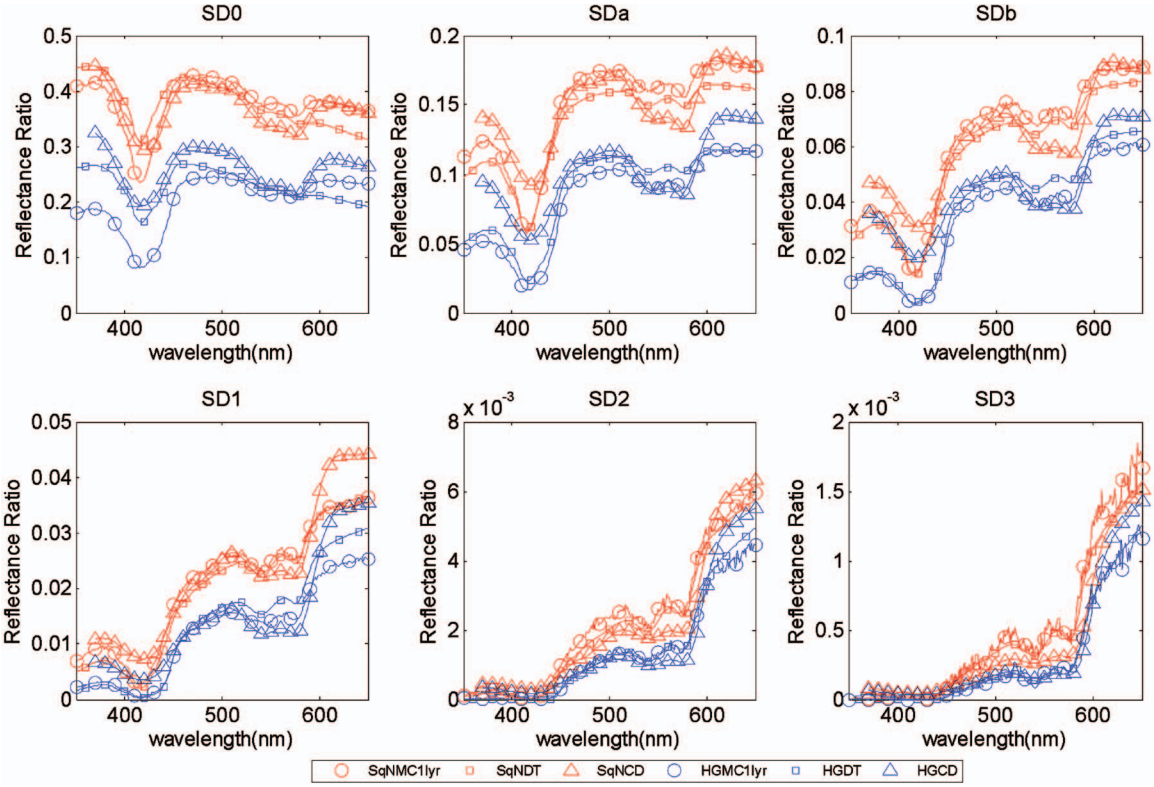

Fig. 5 Validation of one-layer MC and diffusion-based models against *in vivo* clinical measurements for both squamous normal and high grade. Spectra are normalized at emission wavelength of 500 nm to an average of the SqN and HG forward models. SqNCD is the SqN clinical data and HGCD is the HG clinical data.

for each wavelength. The standard deviation of the three simulations was orders of magnitude lower than the average. As the results in Fig. 4 indicate, at the source-detector (SD) separation values measured here, the epithelium makes minimal contribution to the detected signal. All further reflectance modeling was done assuming tissue could be described as a single layer with optical properties of stroma.

Figure 4 compares the results of the MC models to the two analytical models of reflectance at each source-detector separation. The diffusion theory forward model is used to set the scale; normalization occurs at 500 nm. A scale factor is determined for the normal and high-grade cases separately and the average of the two is used to scale the MC and P_3-Hybrid spectra. All four models are in good agreement for all SD separations, except for SD0. This is expected because for SD0, the transport albedo is low and the SD separation is only 0.25 mm. Because both forward models adequately describe the shape of the MC simulations with good agreement, the simpler diffusion-based model was chosen for further analysis.

Figure 5 compares the results of the one-layer MC simulation, the diffusion theory forward model, and the average clinical data for both squamous normal and high-grade precancer. For clarity, the standard deviation of the average clinical data is not shown in Fig. 5, but for reference, the standard deviation for the squamous normal clinical data at 500 nm for SD1 is 0.0134. Again, except for SD0 (SD separation 0), the models and clinical data are in good agreement and show separation between spectra of normal tissue and high-grade precancer.

In order to validate that reflectance spectra could be fit to this analytical expression to accurately extract tissue optical properties, spectra generated using MC simulations were fit to this expression. The parameters extracted from the inverse model fit to the MC simulation were compared to the input parameters of the MC simulation. Figure 6 shows the fits to the MC simulations for SDa, SDb, SD1, SD2, and SD3 for squamous normal as well as high-grade input parameters. The extracted parameters are plotted in Fig. 7. The median value of the percent difference between input and output spectra for all the extracted parameters is 10.6%; parameters extracted from the inverse model capture the expected differences between squamous normal tissue and high-grade precancer.

The inverse reflectance model was used to fit 748 clinical measurements of tissue reflectance. The fit parameters were the volume fraction of blood $[v_f(\text{blood})]$, the hemoglobin oxygen saturation $[O_2\text{Sat}]$, the concentration of structural protein ([protein]), and two constants describing the strength (A) and shape (b) of the scattering in the stroma. Using these parameters as input, the fluorescence model was applied to extract the remaining fluorescence parameters. Box plots of selected extracted parameters are shown in Fig. 8. The clinical data are separated into five groups based on the type of tissue and stage of disease for the measurement: squamous normal, mixed squamous and columnar normal, columnar normal, all tissue types with CIN2, and all tissue types with CIN3 or

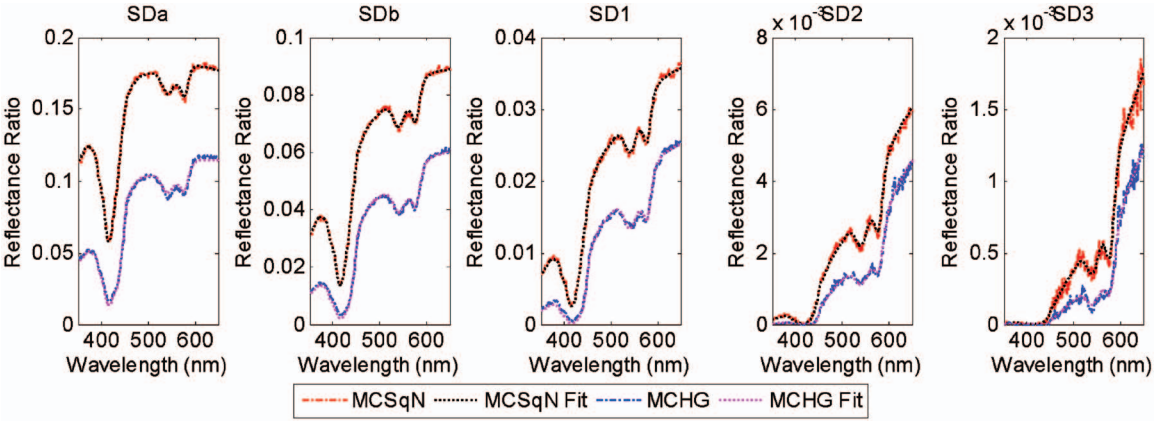

Fig. 6 Results of applying the inverse model to the MC-generated spectra for both squamous normal and high-grade input parameters at source-detector separations greater than SD0. The fit is extremely good in all cases.

cancer. Figure 8(a) shows the median epithelial scattering coefficient; this parameter increases from squamous normal to high-grade disease, but is also increased in columnar tissue. Figure 8(b) shows the concentration of protein in the stroma; squamous normal tissue has lower concentrations of protein, whereas both columnar tissue as well as high grade precancer have higher stromal protein concentrations. Figure 8(c) shows the concentration of keratin in the epithelium; it is higher in squamous normal than in columnar tissue and precancer. Figure 8(d) shows the concentration of NADH in the epithelium; the concentration is higher in columnar tissue than in squamous normal and precancer.

Using fivefold cross-validation, a simple linear discriminant classification algorithm was developed and used to classify the measurements based on the extracted inverse adjoint model parameters as features. The resulting receiver operating characteristic (ROC) curve is shown in Fig. 9. An ROC curve was also generated for a per-patient classification. These curves were generated using the worst diagnosis based on pathology as the gold standard and the highest posterior probability from the classification algorithm as the prediction. To compare the diagnostic performance of the adjoint model parameters to empirical parameters, the ROC curve achieved using principal components (PCs) of the spectra is also

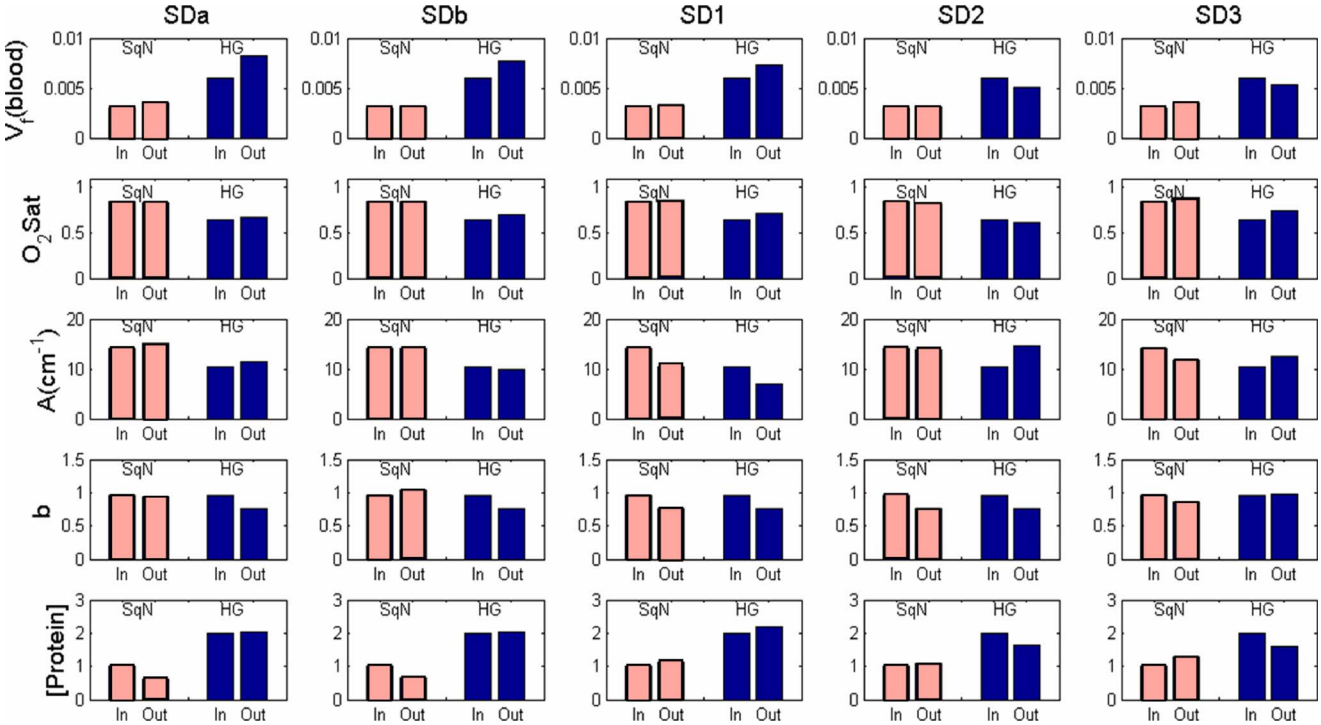

Fig. 7 Comparison of extracted optical properties after fitting the Monte Carlo generated spectra with known input optical properties. The model captures the increase in absorption with disease, both with increase in V_f(blood) and increase in [protein]. The decrease in scattering is also evident by a decrease in A as well as a decrease in O_2Sat. The trends are consistent for all five source-detector separations evaluated.

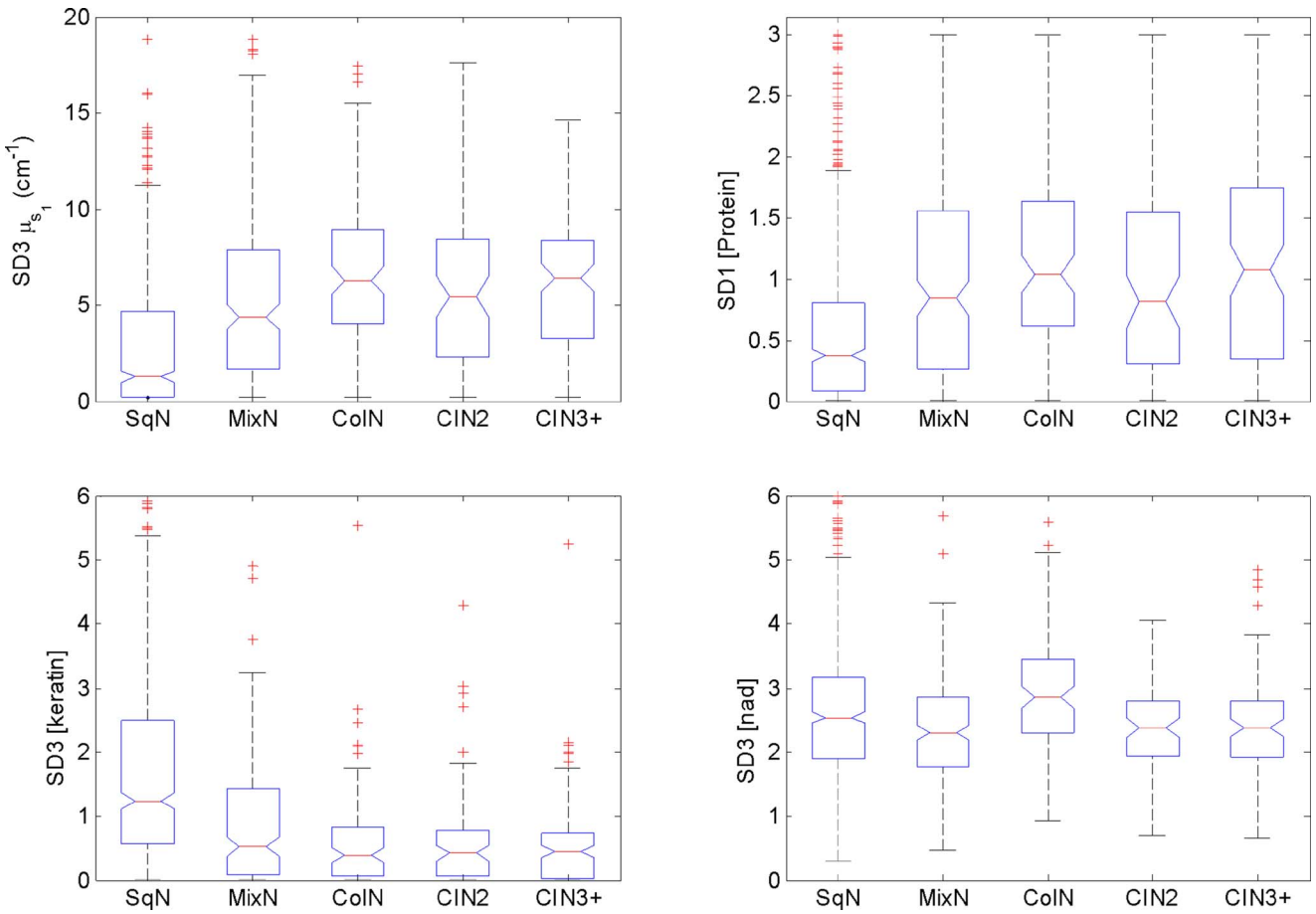

Fig. 8 Example boxplots of optical properties extracted from *in vivo* clinical data. Scale chosen may exclude some outliers. The categories shown are squamous normal (SqN), mixed squamous and columnar normal (MixN), columnar normal (ColN), grade 2 cervical intraepithelial neoplasia (CIN2), and grade 3 cervical intraepithelial neoplasia and cancer (CIN3+): (a) μ_s from the epithelium extracted from the fluorescence spectra, (b) [Protein] from the stroma extracted from the reflectance spectra, (c) [keratin] extracted from the fluorescence spectra, and (d) [NADH] extracted from the fluorescence spectra.

shown. Also plotted in Fig. 9 are the sensitivity and specificities for selected spectroscopy and imaging studies reported in Ref. 11.

7 Discussion and Conclusions

The adjoint reflectance and fluorescence model presented here provides a means to interpret the detected spectroscopic changes associated with neoplastic progression. The model accurately extracts twelve parameters; five from the reflectance spectra and seven from the fluorescence spectra. The reflectance parameters are the volume fraction of blood, the hemoglobin oxygen saturation, the concentration of structural protein, and two constants describing the strength and shape of the scattering in the stroma. The fluorescence parameters include the scattering coefficient of the epithelium and six fluorophores concentrations: NADH, FAD, keratin, and three types of collagen. By extracting these parameters from *in vivo* clinical data, an understanding of the biochemical changes occurring with neoplastic progression can be realized.

In addition, the optical properties extracted with the adjoint model can be used for classification of lesions. In order to evaluate the use of the adjoint model parameters as classification features the performance of the classification algorithm using the adjoint model parameters was compared to the performance if principle components were used as features instead. The per measurement classification performance was better for the adjoint model parameters than for principle components for our data set (Fig. 9). This implies that the model extracts parameters that are biologically significant without giving up diagnostic potential available by empirical means of data reduction. Physically based models that are valid for shorter SD separations, including SD0, are needed to fully capitalize on the data available from this study. The signal from the shorter SD separations might also lead to better discrimination of normal and abnormal tissues.

Reported results of five other studies of optical spectroscopy in the cervix are plotted in Fig. 9 for comparison to our results.[4,26–29] Chang et al. reported a sensitivity and specificity of 83/80% per patient in an analysis of subsets of data from a phase II trial; the analysis results were based on 161 patients using combined reflectance and fluorescence spectroscopy.[26] Georgakoudi et al. reported a sensitivity and specificity of 92/71% per site in a combined reflectance and fluorescence spectroscopy pilot study involving 44 patients.[4] Ferris et al. reported a sensitivity and specificity of 97/70% per patient in a multispectral phase I trial.[27] DeSantis et al. reported a sen-

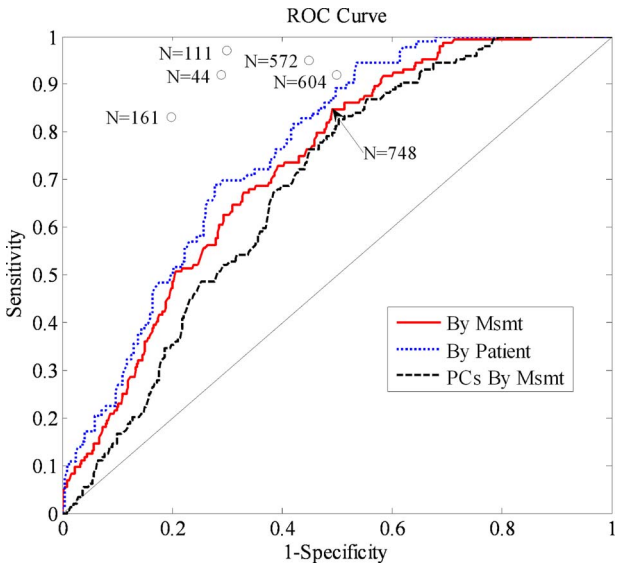

Fig. 9 ROC curve generated from posterior probability output of linear discriminant analysis-based algorithm performed on 748 measurements from 330 patients. Separate ROC curves are also generated based on the posterior probability of each measurement and each patient. In the case of the patients, the worst diagnosis is used as well as the worst posterior probability. Results from other studies are shown with the number of patients used in the analysis (Ref. 11).

sitivity and specificity of 95/55% per patient in a phase II trial where 572 patients were evaluated.[28] Huh et al. reported a sensitivity and specificity of 92/50% per patient in a 604 patient phase II trial using wide-field multispectral imaging.[29] In general, diagnostic performance decreases as the study sample size increases. In our study, the sensitivity and specificity achieved relative to a per measurement gold standard of histopathology are 85/51%; this is increased slightly to 85/53% for a per patient diagnosis. These classification results compare favorably to other studies of optical technologies for detection of cervical cancer and its precursors.

Acknowledgments

This research was supported by National Institutes of Health-National Cancer Institute (NIH-NCI) Program Project Grant No. PO1-CA82710. This work was also supported in part by the Rice Computational Research Cluster funded by NSF under Grant No. CNS-0421109, and a partnership between Rice University, AMD and Cray.

References

1. J. R. Mourant, I. J. Bigio, J. Boyer, R. L. Conn, T. Johnson, and T. Shimada, "Spectroscopic diagnosis of bladder cancer with elastic light scattering," *Lasers Surg. Med.* **17**(4), 350–357 (1995).
2. W. S. Glassman, C. H. Liu, G. C. Tang, S. Lubicz, and R. R. Alfano, "Ultraviolet excited fluorescence spectra from non-malignant and malignant tissues of the gynecological tract," *Lasers Life Sci.* **5**, 49–58 (1992).
3. N. Ramanujam, M. Follen Mitchell, A. Mahadevan-Jansen, S. L. Thomsen, G. Staerkel, A. Malpica, T. Wright, N. Atkinson, and R. Richards-Kortum, "Cervical precancer detection using a multivariate statistical algorithm based on laser induced fluorescence spectra at multiple excitation wavelengths," *Photochem. Photobiol.* **6**, 720–735 (1996).
4. I. Georgakoudi, E. E. Sheets, M. G. Muller, V. Backman, C. P. Crum, K. Badizadegan, R. R. Dasari, and M. S. Feld, "Trimodal spectroscopy for the detection and characterization of cervical precancers *in vivo*," *Am. J. Obstet. Gynecol.* **186**(3), 374–382 (2002).
5. M. Coppleson, B. L. Reid, V. Skladnev, and J. C. Dalrymple, "An electronic approach to the detection of precancer and cancer of the uterine cervix: A preliminary evaluation of polar probe," *Int. J. Cancer* **4**, 79–93 (1994).
6. R. M. Cothren, M. V. Sivak, J. Van Dam, R. E. Petras, M. Fitzmaurice, J. M. Crawford, J. Wu, J. F. Brennan, R. P. Rava, R. Manoharan, and M. S. Feld, "Detection of dysplasia at colonoscopy using laser induced fluorescence: A blinded study," *Gastrointest. Endosc.* **44**, 168–176 (1996).
7. G. Zonios, L. T. Perelman, V. Backman, R. Manoharan, M. Fitzmaurice, J. Van Dam, and M. S. Feld, "Diffuse reflectance spectroscopy of human adenomatous colon polyps *in vivo*," *Appl. Opt.* **38**(31), 6628–6637 (1999).
8. R. R. Alfano, G. C. Tang, A. Pradham, W. Lam, D. S. J. Choy, and E. Opher, "Fluorescence spectra from cancerous and normal human breast and lung tissues," *IEEE J. Quantum Electron.* **23**(10), 1806–1811 (1987).
9. T. Vo-Dinh, M. Panjehpour, B. F. Overholt, C. Farris, F. P. Buckley, and R. Sneed, "*In vivo* cancer diagnosis of the esophagus using differential normalized fluorescence (DNF) indices," *Lasers Surg. Med.* **16**, 41–47 (1995).
10. R. R. Alfano, B. B. Das, J. Cleary, R. Prudente, and E. J. Celmer, "Light sheds light on cancer—distinguishing malignant tumors from benign tissues and tumors," *Bull. N. Y. Acad. Med.* **67**, 143–150 (1991).
11. M. Cardenas-Turanzas, J. A. Freeberg, J. L. Benedet, E. N. Atkinson, D. D. Cox, R. Richards-Kortum, C. MacAulay, M. Follen, and S. B. Cantor, "The clinical effectiveness of optical spectroscopy for the *in vivo* diagnosis of cervical intraepithelial neoplasia: Where are we?," *Gynecol. Oncol.* **107**, 138–146 (2007).
12. N. Ramanujam, M. Follen Mitchell, A. Mahadevan, S. Thomsen, A. Malpica, T. Wright, N. Atkinson, and R. Richards-Kortum, "Spectroscopic diagnosis of cervical intraepithelial neoplasia (CIN) *in vivo* using laser induced fluorescence spectra at multiple excitation wavelengths," *Lasers Surg. Med.* **19**, 63–74 (1996).
13. N. Ramanujam, M. F. Mitchell, A. Mahadevan, S. Thomsen, E. Silva, and R. Richards-Kortum, "*In vivo* diagnosis of cervical intraepithelial neoplasia using 337 nm laser induced fluorescence," *Proc. Natl. Acad. Sci. U.S.A.* **91**, 10193–10197 (1994).
14. N. Ramanujam, M. Follen Mitchell, A. Mahadevan, S. Thomsen, A. Malpica, T. Wright, N. Atkinson, and R. Richards-Kortum, "Development of a multivariate statistical algorithm to analyze human cervical tissue fluorescence spectra acquired *in vivo*," *Lasers Surg. Med.* **19**, 46–62 (1996).
15. C. Brookner, U. Utzinger, G. Staerkel, R. Richards-Kortum, and M. Follen Mitchell, "Cervical fluorescence of normal women," *Lasers Surg. Med.* **24**(1), 29–37 (1999).
16. S. Lam, D. MacAulay, J. Hung, J. LeRiche, A. E. Profio, and B. Palcic, "Detection of dysplasia and carcinoma *in situ* with a lung imaging fluorescence endoscope device," *J. Thorac. Cardiovasc. Surg.* **105**(6), 1035–1040 (1993).
17. J. Sun, K. Fu, A. Wang, A. W. H. Lin, U. Utzinger, and R. Drezek, "Influence of fiber optic probe geometry on the applicability of inverse models of tissue reflectance spectroscopy: Computational models and experimental measurements," *Appl. Opt.* **45**, 8152–8162 (2006).
18. E. L. Hull and T. H. Foster, "Steady-state reflectance spectroscopy in the P_3 approximation," *J. Opt. Soc. Am. A* **18**, 584–599 (2001).
19. G. M. Palmer and N. Ramanujam, "Monte Carlo-based inverse model for calculating tissue optical properties. Part I: Theory and validation on synthetic phantoms," *Appl. Opt.* **45**, 1062–1071 (2006).
20. R. Reif, O. A'Amar, and I. Bigio, "Analytical model of light reflectance for extraction of the optical properties in small volumes of turbid media," *Appl. Opt.* **46**(29), 7317–7328 (2007).
21. D. Arifler, C. MacAulay, M. Follen, and R. Richards-Kortum, "Spatially resolved reflectance spectroscopy for diagnosis of cervical precancer: Monte Carlo modeling and comparison to clinical measurements," *J. Biomed. Opt.* **11**(6), 064027 (2006).
22. S. K. Chang, D. Arifler, R. Drezek, M. Follen, and R. Richards-Kortum, "Analytical model to describe fluorescence spectra of normal and preneoplastic epithelial tissue: comparison with Monte Carlo simulations and clinical measurements," *J. Biomed. Opt.* **9**(3), 511–522 (2004).

23. C. Balas, "A novel optical imaging method for the early detection, quantitative grading, and mapping of cancerous and precancerous lesions of cervix," *IEEE Trans. Biomed. Eng.* **48**(1), 96–104 (2001).
24. J. A. Freeberg, D. M. Serachitopol, N. McKinnon, R. Price, E. N. Atkinson, D. D. Cox, C. MacAulay, R. Richards-Kortum, M. Follen, and B. Pikkula, "Fluorescence and reflectance device variability throughout the progression of a phase II clinical trial to detect and screen for cervical neoplasia using a fiber optic probe," *J. Biomed. Opt.* **12**(3), 034015 (2007).
25. N. M. Marin, M. Follen, and R. Richards-Kortum, "Calibration standards for multi-center clinical trials of fluorescence spectroscopy for *in vivo* diagnosis," *J. Biomed. Opt.* **11**(1), 014010 (2006).
26. S. K. Chang et al., "Combined reflectance and fluorescence spectroscopy for *in vivo* detection of cervical pre-cancer," *J. Biomed. Opt.* **10**, 024031 (2005).
27. D. G. Ferris et al., "Multimodal hyperspectral imaging for the noninvasive diagnosis of cervical neoplasia," *J. Low Genit. Tract Dis.* **5**, 65–72 (2001).
28. T. DeSantis et al., "Spectroscopic imaging as a triage test for cervical disease: a prospective multicenter clinical trial," *J. Low Genit. Tract Dis.* **11**, 18–24 (2007).
29. W. K. Huh et al., "Optical detection of high-grade cervical intraepithelial neoplasia *in vivo*: results of a 604-patient study," *Am. J. Obstet. Gynecol.* **190**, 1249–1257 (2004).